Electrochimica Acta 55 (2010) 1971–1977

Contents lists available at ScienceDirect

Electrochimica Acta

journal homepage: www.elsevier.com/locate/electacta

Non-enzymatic hydrogen peroxide detection using gold nanoclusters-modified phosphorus incorporated tetrahedral amorphous carbon electrodes

Aiping Liu[a,b,c,*], Wenjun Dong[a], Erjia Liu[c], Weihua Tang[a], Jiaqi Zhu[b], Jiecai Han[b]

[a] Department of Physics, Center for Optoelectronics Materials and Devices, Zhejiang Sci-Tech University, Xiasha College Park, Hangzhou 310018, China
[b] Center for Composite Materials, Harbin Institute of Technology, Post-box 3010, Yikuang Street 2, Nangang District, Harbin 150080, China
[c] School of Mechanical and Aerospace Engineering, Nanyang Technological University, 50 Nanyang Avenue, Singapore 639798, Singapore

ARTICLE INFO

Article history:
Received 22 June 2009
Received in revised form 5 November 2009
Accepted 6 November 2009
Available online 13 November 2009

Keywords:
Gold nanocluster
Phosphorus incorporation
Tetrahedral amorphous carbon
Hydrogen peroxide detection
Electrocatalytic activity

ABSTRACT

Sensitive electrochemical electrodes for hydrogen peroxide (H_2O_2) detection were developed using gold nanoclusters (NCs) to modify phosphorus incorporated tetrahedral amorphous carbon films (ta-C:P/Au). Au oxide covered Au NCs were electrodeposited on ta-C:P surfaces, and the size of Au/AuO_x NCs ranged between 50 nm and 91 nm, depending on the deposition time. The ta-C:P/Au electrodes exhibited higher electrocatalytic activity towards H_2O_2 oxidation compared to ta-C:P electrodes. This is due to the three-dimensional island structure of Au/AuO_x NCs, which accelerates electron exchange between ta-C:P and H_2O_2 in phosphate buffered solution. We also found that ta-C:P/Au electrodes with Au/AuO_x NCs of a smaller size and moderate coverage exhibited larger current response to H_2O_2 oxidation. The results obtained from amperometric response curves indicated that the use of Au/AuO_x NCs as microelectrodes directly favored H_2O_2 oxidation through hemispherical diffusion. The linear detection range of H_2O_2 at the non-enzymatic ta-C:P/Au electrodes was identified to be between 0.2 μM and 1 mM with a detection limit of 80 nM under optimized conditions. These ta-C:P/Au electrodes have potential applications in H_2O_2 sensing due to their high sensitivity, fast response and long-term stability.

1. Introduction

The detection of hydrogen peroxide (H_2O_2) has attracted considerable attention, particularly in physiological and biomedical studies and in the monitoring of biological processes. This is because H_2O_2 is a reactive oxygen species and also a by-product of many oxidative biological reactions [1]. Many studies on this subject involved the use of glucose oxidase [2,3]. However, the instability of enzymatic activity, due to factors such as temperature, pH and oxygen, restricts the use of enzyme-based sensors [4]. Thus, we propose using a non-enzymatic electrode for H_2O_2 detection. Carbon materials are regarded to be superior to noble metals due to their low cost, wide potential window and relatively inert electrochemistry in both aqueous and non-aqueous media. Thus, they have potential applications in both biological electrochemistry and industrial electrochemistry [5–10]. The properties of carbon those are important to its use as an electrode material depend on its structural and chemical stability and C–C bond hybridization. For example, highly oriented pyrolytic graphite, glassy carbon and "graphitized" carbon black composed of sp^2 hybridized carbon atoms are usually made under high temperature and pressure, and they have excellent conductivity and electrocatalytic activity. Carbon nanotubes used for electrochemistry are generally in the form of bundles with various sizes, which limits their broad electrochemical application as a single nanoelectrode [6]. Diamond offers distinct properties compared to the "classical" carbon materials (graphite, glassy carbon, and carbon black) and has attracted considerable interest due to its excellent electrochemical properties such as long-term stability, chemical inertness, wide potential window and low background current [7,9–11]. Diamond-like carbon (DLC) or tetrahedral amorphous carbon (ta-C) film is a disordered material consisting of sp^2 and sp^3 hybridized carbon atoms. The sp^3 fraction of ta-C film made by a filtered cathodic vacuum arc system may be as high as 85–90%. The ta-C films are therefore nearly completely sp^3 hybridized with the tetrahedral bonding of diamond and show comparatively high hardness, excellent biocompatibility, chemical inertness, low friction and wear, and high corrosion resistance [12]. Similar to diamond, ta-C film has a large electrical resistivity (10^6–10^8 Ω cm) and usually requires impurity doping to provide sufficient conductivity for electrochemistry. When ta-C or DLC films are doped with nitrogen (ta-C:N), phosphorus (ta-C:P) or Ni (DLC:Ni), they have been shown to be inexpensive, easily fabricated and reproducible materials. These conductive carbon films possess low double layer capacitance, a large potential

* Corresponding author at: Department of Physics, Center for Optoelectronics Materials and Devices, Zhejiang Sci-Tech University, Xiasha College Park, Hangzhou 310018, China. Tel.: +86 571 86843468; fax: +86 571 86843468.
E-mail address: liuaiping1979@gmail.com (A. Liu).

0013-4686/$ – see front matter © 2009 Elsevier Ltd. All rights reserved.
doi:10.1016/j.electacta.2009.11.017

window, low background current, stability in challenging environments, comparative electrocatalysis and high resistance to product adsorption and do not require a non-activation treatment of the electrode surface by polishing, heating or laser activation. With ambient temperature growth on virtually any substrate and smooth surfaces, doped ta-C or DLC films exhibit many advantages over the difficult-to-nucleate, high-temperature growth boron-doped diamond (BDD) films and "classical" carbon materials and are regarded as an appropriate material for electroanalytical applications [5,8,12–20].

However, the electrocatalytic activity of doped ta-C electrodes for H_2O_2 electro-oxidation is still limited. Metal nanoparticles (NPs) or nanoclusters (NCs), with large surface areas and good electronic properties, show good performance in accumulating charge and in improving the electrochemical response of electrodes in electrochemical sensors and biosensors [21–24]. These metal NPs or NCs, such as Au NPs or NCs, may be partially oxidized in aqueous media [25], and the oxidation products often act as the mediators for the reduction and oxidation of dissolved species in solution [26,27]. Metallic modification of carbon electrodes has been carried out to improve the electrocatalytic activity for H_2O_2 oxidation in the past few years. For example, You et al. developed a H_2O_2 detector using a graphite-like carbon film electrode containing 6.5% platinum NPs [28]. Ivandini et al. fabricated Pt-modified diamond electrodes by implantation method to oxidize H_2O_2 [29]. Chikae et al. fabricated Au and Pt NPs on screen-printed carbon strips using an electrodeposition process and confirmed the electrocatalytic activities of the electrodes in H_2O_2 oxidation [30]. Hrapovic et al. reported the enhanced activity of Pt NPs modified carbon nanotubes towards H_2O_2 oxidation or reduction due to the catalytic action of Pt NPs [31]. To our knowledge, there were few reports on H_2O_2 oxidation with metal NPs- or NCs-modified conductive ta-C electrodes. In this paper, Au NCs-modified ta-C:P (ta-C:P/Au) films were fabricated and the Au deposits were characterized by scanning electron microscopy (SEM). The capability of ta-C:P/Au films as analytical electrodes for H_2O_2 detection was investigated by voltammetric and amperometric methods. The kinetics of H_2O_2 oxidation at ta-C:P/Au electrodes was also examined in detail.

2. Experimental

2.1. Reagents

H_2O_2 solution (30%) and $HAuCl_4 \cdot 3H_2O$ (purity 99.99%) were supplied by Sigma (USA). All other chemicals were of analytical grade. Water was obtained from a Millipore Q purification system (resistivity > 18 MΩ cm). 0.2 M phosphate buffered solutions (PBS, pH = 5.0–10.0) were prepared by combining appropriate volumes of 0.2 M NaH_2PO_4 and 0.2 M Na_2HPO_4 solutions.

2.2. Preparation of ta-C:P/Au electrodes

Using a filtered cathodic vacuum arc system with 10-sccm phosphine (purity 99.9999%) as the dopant source, 80-nm ta-C:P films were deposited on p-type silicon wafers (ρ = 0.01–0.02 Ω cm) [14]. Au NCs were electrodeposited on as-prepared ta-C:P surfaces in a 0.1 M H_3BO_4 solution containing 0.5 mM $HAuCl_4$ (the pH of the solution was adjusted to 1.5 with dense H_2SO_4) using an electrochemical workstation (CHI 660A, China) [32]. The potential was scanned from 0.85 V to −0.05 V (*vs.* saturated calomel electrode (SCE)) and back to 0.85 V for 20 s, 180 s, 360 s and 720 s at a scan rate of 0.02 V s^{-1} under nitrogen bubbling conditions. These ta-C:P/Au samples were correspondingly labeled as ta-C:P/Au_1 to ta-C:P/Au_4 as the deposition time increased from 20 s to 720 s. The three-electrode system consisted of either a ta-C:P or a ta-C:P/Au working electrode, a SCE reference electrode and a Pt foil counter electrode. The edges and back of the ta-C:P and ta-C:P/Au electrodes were sealed by an O-ring resin with an apparent geometric surface area (A_g) of 0.4 cm^2. The as-prepared ta-C:P/Au electrodes were then cycled in 0.1 M H_2SO_4 solution until a stable voltammogram was achieved, indicating complete cleaning of Au active areas.

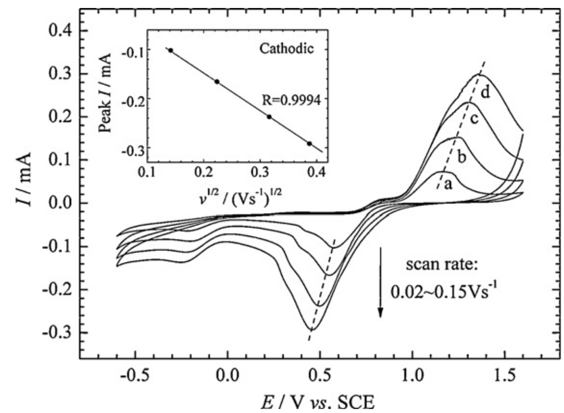

Fig. 1. Cyclic voltammograms of the ta-C:P/Au_1 electrode in a 0.1 M H_2SO_4 solution at different scan rates. Inset is the dependence of the peak current of Au reduction on the square root of the scan rate.

2.3. Characterization of ta-C:P/Au electrodes

The composition of the ta-C:P film was measured by X-ray photoemission spectroscopy using a PHI ESCA 5700 spectrometer with an Al Kα line (1486.6 eV) as the X-ray source. The content of phosphorus (P/(C + P)) in the ta-C:P film was calculated to be 6.8 at.% from the core level spectra of P 2p and C 1s using the sensitivity factors of the instrument [14]. The deposition process of Au was analyzed by cyclic voltammetry in a 0.1 M H_2SO_4 solution at different scan rates. Au NCs were examined using a Hitachi S4800 SEM. The electrochemical behavior of the $Fe(CN)_6^{3-/4-}$ redox couple at ta-C:P and ta-C:P/Au electrodes were investigated in a 5 mM $K_3Fe(CN)_6$ and 1 M KCl solution at 0.02 V s^{-1}. H_2O_2 detection using ta-C:P and ta-C:P/Au electrodes was performed in 0.2 M PBS with different pHs using the three-electrode system described above. In steady-state amperometric experiments, an optimal potential was selected with a stirring rate of 200 rpm, and the current–time curves were recorded after a constant background current was established. Electrolyte solutions were purged with high-purity nitrogen during electrochemical experiments. The kinetics of H_2O_2 oxidation at ta-C:P and ta-C:P/Au electrodes was estimated by cyclic voltammetry and amperometric measurement. All electrochemical experiments were carried out at 25 °C using a thermostated water jacket.

3. Results and discussion

3.1. Characterization of Au NCs

Fig. 1 shows the cyclic voltammograms (CVs) of the ta-C:P/Au_1 electrode in a 0.1 M H_2SO_4 solution at different scan rates. A reduction peak of Au was observed at about 0.58 V in the negative scan of Curve a, and the peak at −0.18 V was due to the reduction of hydrogen ions to hydrogen atoms [33]. The peak at 1.16 V on the returning curve was verified to be the oxidation peak of Au deposited on the ta-C:P surface. Furthermore, the reduction peak and oxidation peak of Au shifted cathodically and anodically, respectively, with increasing sweep rates. The linear relationship between the reduction peak current and the square root of sweep rate, ν (correlation

Table 1
Parameters of ta-C:P/Au electrodes obtained from SEM and voltammetry analyses. The related error for all values is less than 5%.

Sample	A_{Au} (cm^2)	Diameter of Au/AuO$_x$ NCs (nm)	Density of Au/AuO$_x$ NCs (units cm^{-2})	Θ	Θ_R	A_U (cm^2)	Γ (mol cm^{-2})	ΔE_p (V)	i_p^{ox}/i_p^{red}
ta-C:P/Au$_1$	0.08	50.1	2.3×10^9	0.045	0.040	0.384	2.76×10^{-10}	0.076	0.94
ta-C:P/Au$_2$	0.15	51.7	5.9×10^9	0.124	0.120	0.352	5.20×10^{-10}	0.066	0.97
ta-C:P/Au$_3$	0.23	58.7	5.1×10^9	0.138	0.130	0.348	7.94×10^{-10}	0.063	0.98
ta-C:P/Au$_4$	0.35	90.1	4.0×10^9	0.255	0.225	0.310	1.21×10^{-9}	0.063	0.99

Aiping Liu et al.

coefficient, $R = 0.9994$) indicated that the reduction process of Au was diffusion-controlled (the inset in Fig. 1). The Au oxide formed during the position sweep covered the surface of Au NCs, and could serve as a mediator, providing electrocatalytic activity together with Au [25–27]. The real surface area of Au loading (A_{Au}) can be estimated from the charge consumed in the reduction of the surface oxide monolayer of Au between 0 V and 0.9 V in the cathodic scan, in N_2-saturated 0.1 M H_2SO_4 ($\nu = 0.1$ V s^{-1}). The reported value of 400 μC cm^{-2} [34,35] was used. The calculation results shown in Table 1 indicate that A_{Au} increases with longer deposition time.

The SEM image of the ta-C:P/Au$_2$ electrode shown in Fig. 2A confirms the uniformly discrete nature of Au/AuO$_x$ NCs on a smooth ta-C:P surface. The average diameters of Au/AuO$_x$ NCs for different ta-C:P/Au electrodes were predicted from SEM images using an image analysis software. Results show that the size of Au/AuO$_x$ NCs, prepared at 20 s, ranged between 13.8 nm and 74.3 nm with a mean value of 50.1 nm. After 180 s of electrodeposition, the size of Au/AuO$_x$ NCs varied in a larger range (12.5–75.1 nm) with a 51.7-nm average (Fig. 2A). With deposition time increasing to 360 s and 720 s, the average diameters of Au/AuO$_x$ NCs increased to 58.7 nm and 90.1 nm, respectively. Larger-sized NCs with three-dimensional island structures were also formed after long deposition times (Fig. 2B). These clusters hinted that the growth of some Au sites occurred around the Au seeds deposited previously. The densities of Au/AuO$_x$ NCs on ta-C:P surfaces were estimated from the SEM images and listed in Table 1. It is clear that the dispersion of Au/AuO$_x$ NCs, which varies in the range of 10^9 units cm^{-2} geometrical surface area, strongly depends on the deposition time. Smaller NCs tended to merge and form larger ones due to the overlap of these NCs after long deposition times. This could result in a decrease in the density of Au/AuO$_x$ NCs. According to the theory of Davies et al. [36], the global coverage of Au/AuO$_x$ NCs, Θ, can be estimated by using an approximation of monolayer distribution of the NCs:

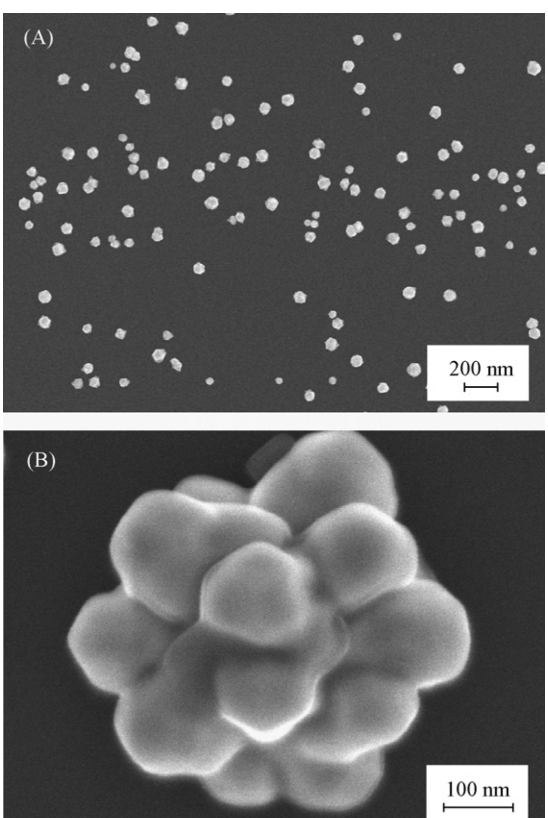

Fig. 2. SEM images of (A) ta-C:P/Au$_2$ and (B) Au/AuO$_x$ NC.

$$\Theta = \frac{\pi R_b^2 N_{gold}}{A_g}, \quad (1)$$

where R_b is the mean radius of Au NCs and N_{gold} is the number of Au NCs deposited on the ta-C:P surface with an area of A_g. The actual area of "uncovered" electrode A_U is given by:

$$A_U = (1 - \Theta_R)A_g \quad (2)$$

where Θ_R is the real coverage of Au/AuO$_x$ NCs and is calculated using the formula:

$$\Theta_R = 1 - e^{-\Theta} \quad (3)$$

Therefore, the real area of ta-C:P/Au electrodes can be obtained from A_{Au} and A_U and the results are shown in Table 1. The surface coverage of Au/AuO$_x$, Γ (mol cm^{-2}), on ta-C:P electrodes can also be determined from the charge (Q) associated with the oxidation of Au deposits by sweeping the potential between 0.9 V and 1.6 V in a N_2-saturated 0.1 M H_2SO_4 solution ($\nu = 0.1$ V s^{-1}) using the following equation [34,37]:

$$\Gamma = \frac{Q}{nFA_g} \quad (4)$$

where n is the stoichiometric number of electrons involved in the electrode reaction and F is the Faraday constant. The data displayed in Table 1 show that higher Au loading results in a larger size of Au/AuO$_x$ NCs and a larger coverage of Au NCs on the ta-C:P surfaces. Θ_R is calculated to be about 0.225 and Γ is 1.21 nmol cm^{-2} after 720 s of deposition. This Γ value is less than the amount of Au in an Au (1 1 1) monolayer surface (2.5 nmol cm^{-2}) [34]. A continuous Au film is therefore not formed after 720 s of deposition.

Fig. 3A shows the electrochemical behavior of different electrodes in 5 mM $K_3Fe(CN)_6$ and 1 M KCl solution at a scan rate of 0.02 V s^{-1}. The ta-C:P electrode exhibits a nonreversible behavior with a peak potential difference (ΔE_p) of 0.15 V and peak current density ratio (i_p^{ox}/i_p^{red}) of 0.90. Comparably, ta-C:P/Au electrodes possess quasi-reversibility towards the $Fe(CN)_6^{3-/4-}$ redox reaction and their catalytic capability is dependent on the Au coverage on the electrode surface, as displayed in Table 1. The results indicate that the reversibility of the ta-C:P/Au electrodes is improved after three-dimensional Au/AuO$_x$ NCs modification, resulting in an enhancement of electrochemical activity.

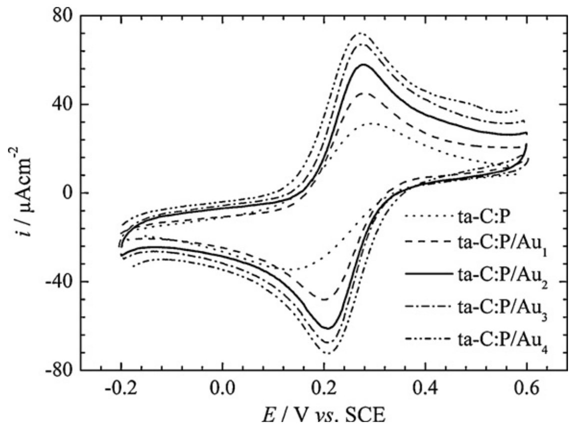

Fig. 3. Cyclic voltammograms of ta-C:P and ta-C:P/Au electrodes in 5 mM $K_3[Fe(CN)_6]$ and 1 M KCl solution at 0.02 V s^{-1}.

3.2. H_2O_2 detection using ta-C:P and ta-C:P/Au electrodes

3.2.1. Voltammetric responses of H_2O_2 on ta-C:P and ta-C:P/Au electrodes

Fig. 4A shows the CVs obtained using the ta-C:P electrode in 0.2 M PBS (pH 7.4) with and without 1 mM of H_2O_2 at a scan rate of 0.1 V s^{-1}. A prominent H_2O_2 oxidation peak (Peak A) was observed at 0.78 ± 0.08 V (Curve b). The response current of H_2O_2 obtained using ta-C:P may contribute to the catalysis action of active CP sites on the ta-C:P surface [14]. Fig. 4B shows the CVs of ta-C:P/Au electrodes, with different sizes of Au/AuO_x NCs deposited on them, in 0.2 M PBS (pH 7.4) with 1 mM H_2O_2 at a scan rate of 0.1 V s^{-1}. The two peaks, Peak B at 0.28 V and Peak C at 0.96 V, observed at the ta-C:P/Au_2 electrode in pure PBS, were attributed to the reduction and oxidation peaks of Au deposited on the ta-C:P surface (Curve a). The catalytic current density obtained at the ta-C:P/Au electrodes (Curves b–e) was 3–6 times higher than that obtained at the ta-C:P electrode upon H_2O_2 oxidation. Peaks A obtained at the ta-C:P/Au electrodes shifted to 0.67 ± 0.06 V, which is 0.1 V lower than that obtained at the ta-C:P electrode. The lower oxidation potential and higher current density obtained at the ta-C:P/Au electrodes revealed their higher catalytic abilities towards H_2O_2 oxidation compared to ta-C:P electrodes. This is because the three-dimensional Au/AuO_x NCs accelerate the electron exchange between ta-C:P electrodes and H_2O_2 in aqueous solution. Moreover, the current density of H_2O_2 oxidation depends on the size of Au/AuO_x NCs. When 50.1-nm Au/AuO_x NCs were deposited on the ta-C:P electrode surface, the real surface area of Au NCs on ta-C:P/Au_1 electrode increased. This was accompanied by an increase in the signal to background (S/B) ratio and a decrease in detection potential for H_2O_2 oxidation (Fig. 4B and C). Although the greater surface area of the ta-C:P/Au_1 electrode might result in an increase in the background current, the sensitivity of H_2O_2 detection at the ta-C:P/Au_1 electrode was enhanced by improving the S/B ratio. The Au/AuO_x NCs can be regarded as microelectrodes, uniformly distributed on the ta-C:P surface and a higher detection current can be obtained at each NC. After 180 s of deposition, the size of Au/AuO_x NCs varied in a wider range with a slight increase in the average diameter. The S/B ratio increased due to the increased real surface area of ta-C:P/Au_2. Further lengthening of the deposition time improved the growth of Au/AuO_x NCs and increased the background current, resulting in a decrease in the S/B ratio (Fig. 4C). In an earlier study, Hutton et al. [38] reported that the exchange current density of Pt clusters-modified glassy carbon for hydrogen evolution increased with a decrease in Pt particle size. Jia et al. [39] also found that biosensors fabricated with smaller-sized Au NPs exhibited a larger current response than those prepared with larger-sized Au NPs. The maximum value of S/B is obtained at a ta-C:P/Au_2 electrode with moderate coverage and thus, it was the chosen electrode for the following voltammetric and amperometric measurements.

3.2.2. Effect of pH and detection potential

The effect of pH of the measurement solution on the peak current density obtained at the ta-C:P/Au_2 electrode was investigated (Fig. 5A), since pH is an important factor in the sensitivity, activity and stability of electrodes. It is interesting to note that the voltammetric waves shift negatively when increasing pH from 5.0 to 10.0. This may be attributed to the increase of negative charge on the ta-C:P/Au_2 electrode. The current response to 1 mM H_2O_2 obtained

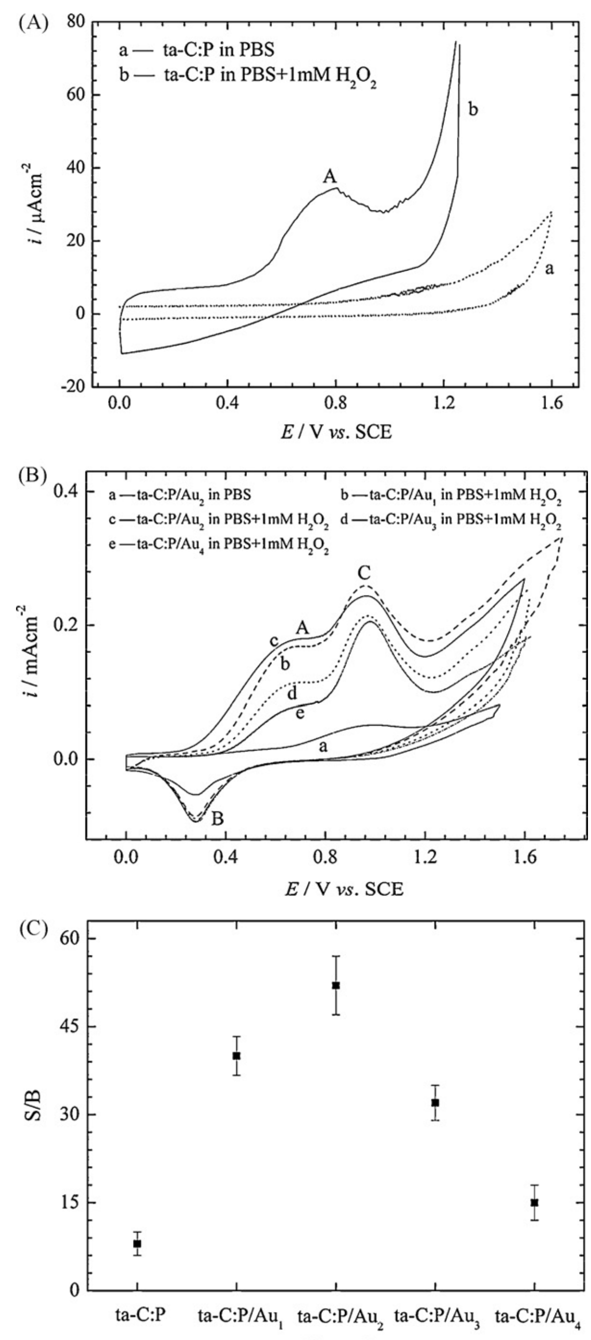

Fig. 4. Cyclic voltammograms of (A) ta-C:P and (B) ta-C:P/Au electrodes in 0.2 M PBS (pH 7.4) with and without 1 mM H_2O_2 at 0.1 V s^{-1}. (C) Signal/background ratios calculated from the cyclic voltammograms of ta-C:P and ta-C:P/Au electrodes in 0.2 M PBS (pH 7.4) with and without 1 mM H_2O_2.

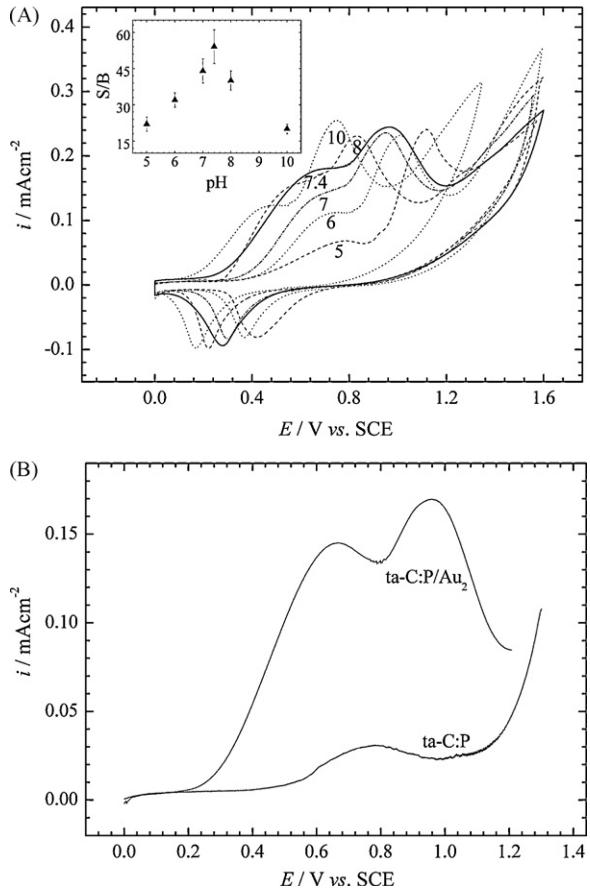

Fig. 5. (A) Cyclic voltammograms of the ta-C:P/Au_2 electrode in 1 mM H_2O_2 and 0.2 M PBS at different pH. Inset is the dependence of signal/background ratio on pH at the ta-C:P/Au_2 electrode in 0.2 M PBS with 1 mM H_2O_2. (B) Evolution of current density difference with the change of potential obtained at ta-C:P and ta-C:P/Au_2 electrodes in 0.2 M PBS (pH 7.4) with and without 1 mM H_2O_2.

at the ta-C:P/Au_2 electrode increased pronouncedly from pH 5.0 to 7.0, changed slightly in the pH region between 7.0 and 8.0, then decreased when pH was greater than 8.0. According to Hall et al. [40], acidic conditions were likely to hinder the formation of the binding site and could result in protonation, producing inactive sites with higher anodic potential. In addition, the contribution of background current at pH 7.4 was very low, in contrast to those observed at other pH values. The maximum S/B ratio was therefore obtained at pH 7.4 (see inset in Fig. 5A). The effect of pH of the measurement solution on the peak current density obtained at the ta-C:P electrode was similar to that obtained at the ta-C:P/Au_2 electrode. Therefore, both ta-C:P and ta-C:P/Au_2 electrodes are suitable for the detection of H_2O_2 at pH 7.4.

Moreover, the difference in current densities due to change in potential obtained at ta-C:P and ta-C:P/Au_2 electrodes in 0.2 M PBS (pH 7.4) with and without 1 mM H_2O_2 was calculated. It can be seen from Fig. 5B that 0.77 V and 0.67 V should be chosen as the optimal measurement potentials for ta-C:P and ta-C:P/Au_2 electrodes to avoid interference from Au oxidation and O_2 evolution.

3.2.3. Amperometric responses of H_2O_2 at ta-C:P and ta-C:P/Au electrodes

Fig. 6A shows typical amperometric response curves of H_2O_2 oxidation at ta-C:P and ta-C:P/Au_2 electrodes using the above optimum conditions (0.77 V detection potential for ta-C:P and 0.67 V for ta-C:P/Au_2, 0.2 M PBS at pH 7.4) with successive increments of H_2O_2, of various volumes and concentrations, in 10 mL PBS. The electrode responses achieved steady-state signals within 8 s. The linear characteristics of the electrodes for H_2O_2 detection can be observed in Fig. 6B. The current density of H_2O_2 oxidation obtained at the ta-C:P electrode was proportional to the H_2O_2 concentration in the range of 2–200 μM, with a sensitivity (change of current density per unit concentration of H_2O_2) of 48.4 ± 0.2 nA cm^{-2}/μM (R = 0.9976). The detection limit, based on the signal-to-noise ratio (S/N = 3), was estimated to be 0.5 ± 0.1 μM. After modification with Au/AuO_x NCs, the current density of H_2O_2 oxidation obtained at the ta-C:P/Au_2 electrode was linear within a wider concentration range from 0.2 μM to 1 mM (R = 0.9988) and had a sensitivity of 293.8 ± 0.3 nA cm^{-2}/μM. The detection limit at S/N = 3 was calculated to be 80 nM. This value was one order of magnitude lower than that obtained at the ta-C:P electrode under the same conditions, and three orders of magnitude lower than that obtained at DLC electrodes (20–30 μM) [8]. When the concentration of H_2O_2 exceeded 1 mM, the current density obtained at the ta-C:P/Au_2 electrode was no longer proportional to the bulk H_2O_2 concentration. The current density of H_2O_2 oxidation saturated at a lower concentration of 300 μM at the ta-C:P electrode. This may be explained by the suggestion that maximum electrode response and sensitivity can only be obtained when oxygen gas (a product of H_2O_2 oxidation) is rapidly removed from the vicinity of the electrode. The postponed diffusion of O_2 from the electrode surface to the solution, and H_2O_2 from the solution to the electrode surface slows down the reaction rate and affects the kinetics of the overall reaction when a large amount of O_2 is created on the electrode surface. As a result, the

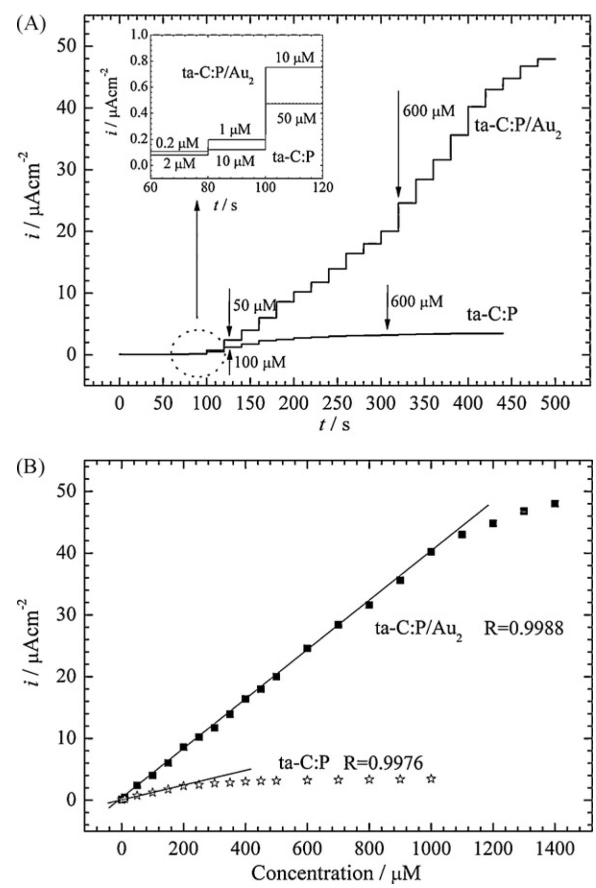

Fig. 6. (A) Current density–time response of H_2O_2 oxidation obtained at ta-C:P and ta-C:P/Au_2 electrodes with successive addition of various volumes and concentrations H_2O_2 into 10 mL 0.2 M PBS (pH 7.4). Electrode potential: 0.77 V *vs.* SCE for ta-C:P and 0.67 V *vs.* SCE for ta-C:P/Au_2. The solution was stirred magnetically during measurements. Inset is the magnification of the dashed part. (B) Relation between the current density of H_2O_2 oxidation and the concentration of H_2O_2 obtained at the ta-C:P and ta-C:P/Au_2 electrodes in 0.2 M PBS (pH 7.4).

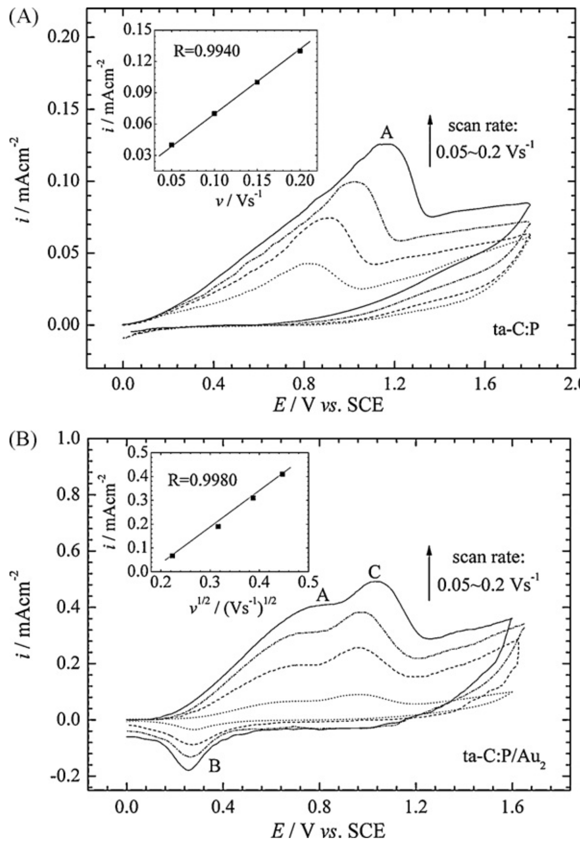

Fig. 7. Cyclic voltammograms of (A) ta-C:P and (B) ta-C:P/Au_2 electrodes in 0.2 M PBS (pH 7.4) with 5 mM H_2O_2 at different scan rates. Inset represents the dependence of peak current density of H_2O_2 oxidation on scan rate or square root of scan rate.

sensitivities of ta-C:P and ta-C:P/Au_2 electrodes are lowered. ta-C:P electrodes with smaller surface area tend to be passivated and ineffective in the presence of lower amounts of O_2 or H_2O_2. ta-C:P/Au_2 electrodes with a larger real surface area and higher ratio of A_{Au} to real surface area preponderates over ta-C:P electrodes in terms of the higher S/B and S/N ratios, and a lower detection limit can therefore be obtained at this electrode.

3.3. Kinetics of H_2O_2 oxidation

The kinetics of H_2O_2 oxidation at ta-C:P and ta-C:P/Au_2 electrodes were estimated by cyclic voltammetry and current–time measurement. Fig. 7 shows the CVs obtained at ta-C:P and ta-C:P/Au_2 electrodes in 0.2 M PBS (pH 7.4), with 5 mM H_2O_2, at different scan rates. The peak position of H_2O_2 oxidation at the ta-C:P electrode obviously shifted towards the positive direction with increasing scan rate. The peak current density of H_2O_2 oxidation was dependent on the scan rate from 0.05 V s^{-1} to 0.2 V s^{-1} (R = 0.9940). The overall process of H_2O_2 oxidation was therefore a surface-controlled electrode process. Thus, an excellent linear relation between the peak current density of H_2O_2 oxidation and the square root of scan rate ($\nu = 0.05$–$0.2\,V\,s^{-1}$) with R = 0.9980 was obtained at the ta-C:P/Au_2 electrode, demonstrating the speedy reaction kinetics and diffusion-controlled process (Fig. 7B).

Fig. 8A shows the current density–time curves obtained at the ta-C:P/Au_2 electrode in 0.2 M PBS (pH 7.4) with and without 1–5 mM H_2O_2. According to the theory of diffusion control, the time (t) dependence of the current (I) for linear diffusion at a planar electrode follows Cottrell's equation [41]:

$$I = nFAD_0^{1/2}C_0^*\pi^{-1/2}t^{-1/2}, \quad (5)$$

where D_0 is the diffusion coefficient and C_0^* is the concentration of the active species. The area A may be the geometric surface area or the real surface area of the electrode, depending on measurement time [34]. Similarly, the time dependence of the current for hemispherical diffusion at a microelectrode is described by the following equation:

$$I = nFAD_0C_0^*(\pi^{-1/2}D_0^{-1/2}t^{-1/2} + 4\pi^{-1}r^{-1}), \quad (6)$$

where r is the radius of the microelectrode. It can be seen from Fig. 8B that the intercepts of the Cottrell plots are not zero and the slopes are small, indicating that the total current density has a small time-independent component. It can be inferred that the kinetics of H_2O_2 oxidation at the ta-C:P/Au_2 electrode is mainly controlled by hemispherical diffusion. The three-dimensional Au/AuO_x NCs not only accelerate the electron exchange between the ta-C:P electrode and H_2O_2 but also directly favors H_2O_2 oxidation as microelectrode arrays on the ta-C:P surface. That is, Au/AuO_x NCs are dispersed on the surface of the ta-C:P electrode in the form of microelectrodes.

3.4. Reproducibility of the ta-C:P/Au electrode

The repeatability of ta-C:P/Au_2 electrode is tested. The relative standard deviation of amperometric current responses recorded by 100 injections of 10 μL of H_2O_2 (1 mM) was found to be 4.5%. The long-term stability of the ta-C:P/Au_2 electrode was investigated over a 60-day period. ta-C:P/Au_2 electrode was stored at 4 °C and measured every 2 days. The electrode's response to H_2O_2 oxidation under identical conditions decreased to 85% of the initial response

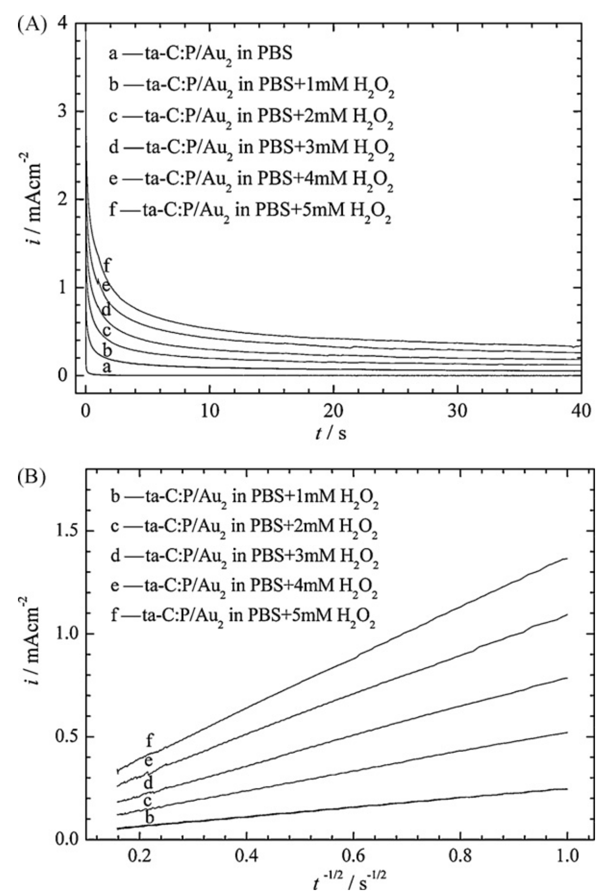

Fig. 8. (A) Amperometric responses of the ta-C:P/Au_2 electrode in 0.2 M PBS (pH 7.4) with and without different concentrations of H_2O_2. (B) Cottrell plots obtained at the ta-C:P/Au_2 electrode in 0.2 M PBS (pH 7.4) with different concentrations of H_2O_2.

after 2 weeks due to the absence of some Au/AuO_x NCs. However, the response maintained at a similar level during a 2-month period thereafter, implying the long-term stability of the electrode.

4. Conclusions

Gold NCs-modified, phosphorus incorporated tetrahedral amorphous carbon (ta-C:P/Au) was fabricated using a filtered cathodic vacuum arc process followed by electrodeposition. The real surface area of ta-C:P/Au electrodes modified with Au/AuO_x NCs increased compared to that of ta-C:P electrodes. The size and coverage of Au/AuO_x NCs can be adjusted by controlling the deposition time. The Au/AuO_x NCs significantly improved the electrochemical activity and reversibility of ta-C:P electrodes towards ferricyanide oxidation reaction and provided high catalytic activity towards hydrogen oxidation (H_2O_2) oxidation due to the action of three-dimensional NCs. The detection limit of H_2O_2 obtained at the ta-C:P/Au electrode with Au/AuO_x NCs of small size and moderate coverage was estimated to be 80 nm, which was one order magnitude smaller than that obtained at the ta-C:P electrode under optimal conditions. The results from current density–time measurement indicated that H_2O_2 oxidation at the ta-C:P/Au electrode was mainly controlled by hemispherical diffusion. Accelerated oxidation of H_2O_2 was induced by Au/AuO_x NCs microelectrodes dispersed on ta-C:P surfaces. The successful detection of H_2O_2 at ta-C:P/Au electrodes implies that the electrodes may be applied as a non-enzymatic H_2O_2-based biosensor due to their immediate response, high sensitivity and good reproducibility.

Acknowledgements

This work is partly supported by the National Natural Science Foundation of China (Grant No. 50902123 and 50972130), the Scientific Research Fund of Zhejiang Provincial Education Department (Grant No. Y200806012) and the Environment and Water Industry Development Council (EWI) of Singapore (Grant No. 0601-IRIS-035-00).

References

[1] J.W. Lee, J.D. Helmann, Nature 440 (2006) 363.
[2] L. Wang, E.K. Wang, Electrochem. Commun. 6 (2004) 225.
[3] J. Wang, J.A. Carlisle, Diamond Relat. Mater. 15 (2006) 279.
[4] S. Park, H. Boo, T.D. Chung, Anal. Chim. Acta 556 (2006) 46.
[5] R.G. Compton, J.S. Foord, F. Marken, Electroanalysis 15 (2003) 1349.
[6] R.L. McCreery, Chem. Rev. 108 (2008) 2646.
[7] T. Tatsuma, H. Mori, A. Fujishima, Anal. Chem. 72 (2000) 2919.
[8] R. Maalouf, H. Chebib, Y. Saikali, O. Vittori, M. Sigaud, F. Garrelie, C. Donnet, N. Jaffrezic-Renault, Talanta 72 (2007) 310.
[9] J.W. Zhao, L.Z. Wu, J.F. Zhi, Analyst 134 (2009) 794.
[10] T. Watanabe, Y. Einaga, Biosens. Bioelectron. 24 (2009) 2684.
[11] A. Hartl, E. Schmich, J.A. Garrido, J. Hernando, S.C.R. Catharino, S. Walter, P. Feulner, A. Kromka, D. Steinmuller, M. Stutzmann, Nat. Mater. 3 (2004) 736.
[12] J. Robertson, Mater. Sci. Eng. R 37 (2002) 129.
[13] N. Menegazzo, C.M. Jin, R.J. Narayan, B. Mizaikoff, Langmuir 23 (2007) 6812.
[14] A.P. Liu, J.Q. Zhu, J.C. Han, H.P. Wu, W. Gao, Electroanalysis 19 (2007) 1773.
[15] M.R. Lockett, S.C. Weibel, M.F. Phillips, M.R. Shortreed, B. Sun, R.M. Corn, R.J. Hamers, F. Cerrina, L.M. Smith, J. Am. Chem. Soc. 130 (2008) 8611.
[16] J.B. Jia, D. Kato, R. Kurita, Y. Sato, K. Maruyama, K. Suzuki, S. Hirono, T. Ando, O. Niwa, Anal. Chem. 79 (2007) 98.
[17] P. Tamiasso-Martinhon, H. Cachet, C. Debiemme-Chouvy, C. Deslouis, Electrochim. Acta 53 (2008) 5752.
[18] A. Zeng, E. Liu, S.N. Tan, S. Zhang, J. Gao, Eletroanalysis 14 (2002) 1294.
[19] K.S. Yoo, B. Miller, R. Kalish, X. Shi, Electrochem. Solid-State Lett. 2 (1999) 233.
[20] S.H. Wan, H.Y. Hu, G. Chen, J.Y. Zhang, Electrochem. Commun. 10 (2008) 461.
[21] M.C. Daniel, D. Astruc, Chem. Rev. 104 (2004) 293.
[22] Y. Song, G.M. Swain, Anal. Chem. 79 (2007) 2412.
[23] G.J. Hutchings, Catal. Today 100 (2005) 55.
[24] B. Hvolbæk, T.V.W. Janssens, B.S. Clausen, H. Falsig, C.H. Christensen, J.K. Nørskov, Nanotoday 2 (2007) 14.
[25] J.P. Sylvestre, A.V. Kabashin, E. Sacher, M. Meunier, J.H.T. Luong, J. Am. Chem. Soc. 126 (2004) 7176.
[26] L.D. Burke, P.F. Nugent, Gold Bull. 31 (1998) 39.
[27] Z. Jia, J. Liu, Y.B. Shen, Electrochem. Commun. 9 (2007) 2739.
[28] T.Y. You, O. Niwa, M. Tomita, S. Hirono, Anal. Chem. 75 (2003) 2080.
[29] T.A. Ivandini, R. Sato, Y. Makide, A. Fujishima, Y. Einaga, Diamond Relat. Mater. 14 (2005) 2133.
[30] M. Chikae, K. Idegami, K. Kerman, N. Nagatani, M. Ishikawa, Y. Takamura, E. Tamiya, Electrochem. Commun. 8 (2006) 1375.
[31] S. Hrapovic, Y.L. Liu, K.B. Male, J.H.T. Luong, Anal. Chem. 76 (2004) 1083.
[32] A.P. Liu, J.Q. Zhu, J.C. Han, H.P. Wu, C.Z. Jiang, Electrochem. Commun. 10 (2008) 827.
[33] A.C. Hill, R.E. Patterson, J.P. Sefton, M.R. Columbia, Langmuir 15 (1999) 4005.
[34] A.J. Bard, L.R. Faulkner, Electrochemical Methods: Fundamentals and Applications, 2nd edition, John Wiley and Sons, New York, 2000.
[35] M.S. El-Deab, T. Okajima, T. Ohsaka, J. Electrochem. Soc. 150 (2003) A851.
[36] T.J. Davies, R.R. Moore, C.E. Banks, R.G. Compton, J. Electroanal. Chem. 574 (2004) 123.
[37] M.R. Miaha, T. Ohsaka, Electrochim. Acta 54 (2009) 1570.
[38] H.D. Hutton, N.L. Pocard, D.C. Alsmeyer, O.J.A. Schueller, R.J. Spontak, M.E. Huston, W.H. Huang, R.L. McCreery, T.X. Neenan, M.R. Callstrom, Chem. Mater. 5 (1993) 1727.
[39] J.B. Jia, B.Q. Wang, A.G. Wu, G.J. Cheng, Z. Li, S.J. Dong, Anal. Chem. 74 (2002) 2217.
[40] S.B. Hall, E.A. Khudaish, A.L. Hart, Electrochim. Acta 44 (1999) 4573.
[41] R.J. Forster, Chem. Soc. Rev. 4 (1994) 289.